TRINET "SHAKEMAPS": RAPID GENERATION OF PEAK GROUND MOTION AND INTENSITY MAPS FOR EARTHQUAKES IN SOUTHERN CALIFORNIA

David J. Wald
U.S. Geological Survey, Pasadena

V. Quitoriano, T. H. Heaton, H. Kanamori
Seismological Laboratory, Caltech, Pasadena

C. W. Scrivner
California Dept. of Conservation, Div. Mines and Geology, Sacramento

ABSTRACT

Rapid (3-5 minutes) generation of maps of ground motion shaking and intensity is accomplished with advances in real-time seismographic data acquisition combined with newly-developed relationships between recorded ground motion parameters and expected shaking intensity values. Estimation of shaking over the entire regional extent of southern California is accomplished by spatial interpolation of the measured ground motions with geologically-based, frequency and amplitude-dependent site corrections. Production of the maps is automatic, triggered by any significant earthquake in southern California. Maps are now made available within several minutes of the earthquake for public and scientific consumption via the World-Wide-Web; they will be made available with dedicated communications for emergency response agencies and critical users.

INTRODUCTION

The most common information available immediately following a damaging earthquake is its magnitude and the epicentral location. However, the damage pattern is not a simple function of these two parameters alone, and more detailed information must be provided to properly ascertain the situation. For example, for the February 9, 1971 earthquake, the northern San Fernando valley was the region with the most damage, even though it was more than 15 km from the epicenter. Likewise, areas strongly affected by the Loma Prieta and Northridge, California, earthquakes that were either distant from the epicentral region or out of the immediate media limelight, were not fully appreciated until long after the initial reports of damage. Most recently, the full extent of damage from the 1995 Kobe, Japan, earthquake was not recognized by the central government in Tokyo until many hours later (e.g., Yamakawa, 1997), delaying rescue and recovery efforts.

As part of the research and development efforts of the TriNet (California Institute of Technology, the California Division of Mines and Geology, and the U. S. Geological Survey) project (see Mori *et al.*, 1998), we have been creating ShakeMap^{TM} for earthquakes (magnitude greater than 3.0) in southern California for the last year (Wald *et al.*, 1997). We currently generate separate maps of the spatial distribution of peak ground motions (acceleration and velocity) as well as a map of instrumentally-derived seismic intensities. These maps provide a rapid portrayal of the extent of potentially damaging shaking following an earthquake and can be used for emergency response, loss estimation, and for public information through the media. Generation of the maps is fully automatic, triggered by any significant earthquake in southern California and made available within

several minutes of the earthquake for public and scientific consumption via the World-Wide-Web; they will be made available with more reliable, dedicated communications for emergency response agencies in the near-future. For example, maps of shaking intensity can be combined with databases of inventories of buildings and lifelines to rapidly produce maps of estimated damage (e.g., Eguchi *et al.*, 1997).

Such maps have traditionally been difficult to produce rapidly and reliably due to limitations of seismic network instrumentation and data telemetry. In addition, adequate relationships between recorded ground motions and damage intensities have only recently been developed, for example, the JMA seismic intensity scale in Japan (Japan Meteorological Agency, 1996). However, with recent advances in digital communication and computation, it is now technically feasible to develop systems to display ground motions in an informative manner almost instantly. A detailed description of the shaking over the entire regional extent of southern California requires interpolation of the measured ground motions. In addition, simple geologically-based, frequency- and amplitude-dependent site corrections factors, currently under development, provide a useful first-order correction for local amplification in areas that are not instrumented. In this report we present ongoing efforts addressing the issues pertinent to rapid ground-motion map-making.

PEAK GROUND MOTION MAPS

The current TriNet seismic station distribution in southern California is shown in Figure 1. The USGS/Caltech stations (triangles) are acquired in real time using a variety of digital telemetry methods (see Mori *et al.*, 1998, for more details). The California Division of Mines and Geology, CDMG, stations (square) are near-real time, utilizing an automated dial-up procedure developed for use with telephone communications (see Shakal *et al.*, 1996, 1998). As of May, 1998, there are 80 USGS/Caltech real-time stations online and nearly 100 CDMG dialup stations; in all there will be approximately 670 TriNet strong-motion stations in the next 3 years. The generation of ShakeMaps is triggered automatically by the event associator for the Southern California Seismic Network (SCSN), operated by the USGS and Caltech. Within the first minute following the shaking, ground motion parameters are available from the USGS/Caltech component of the network and within several minutes most of the important near-source CDMG stations contribute. A more complete CDMG contribution is available approximately within the first half hour. Initial maps are made with just the real-time component of TriNet, but they are updated automatically as more data is acquired. Parametric data from the stations includes PGA and PGV as well as spectral amplitudes (at 3.0 Hz, 1 Hz, and 0.3 Hz).

Shaking maps are prepared by contouring shaking information estimated for every point in a 3-km square grid uniformly sampled throughout southern California. If there were stations at each of the 11,000 grid points, then the creation of shaking maps would be relatively simple. Of course stations are not available for all of these grid points, and in many cases grid points may be tens of kilometers from the nearest reporting station. The overall mapping philosophy is to combine information from individual stations, geology (e.g., soil versus rock), and the distance to the centroid to create the best composite map. The procedure must produce reasonable estimates at grid points located far from available data, while preserving the detailed shaking information available for regions where there are nearby stations. That is, we want the procedure to return the actual data values for stations where there is data.

To determine the strong motion "centroid" (Kanamori, 1993), we apply empirically-derived station site corrections and then fit the observed ground motions to find the best equivalent point-source latitude, longitude, and magnitude. We scan the parameter space to determine the global minimum solution for location and magnitude, and then refine the solution using the method of

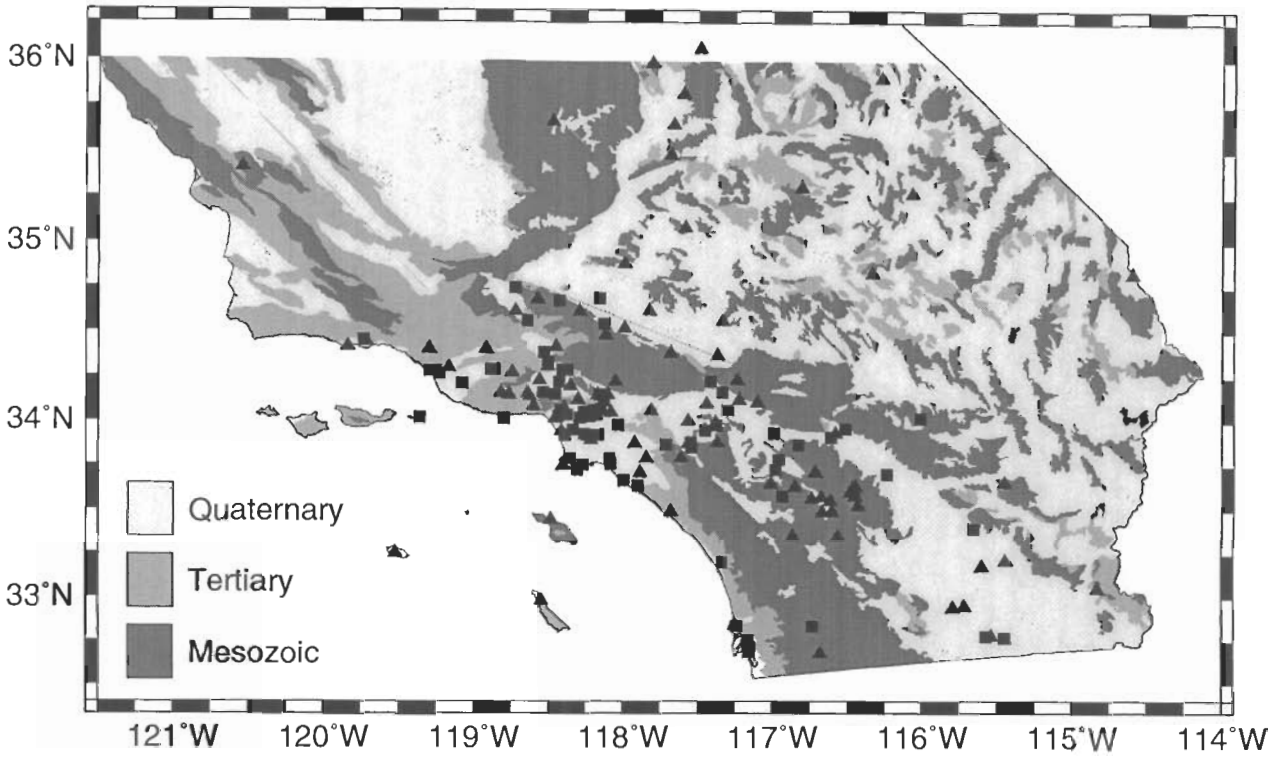

Figure 1: Map of southern California showing current TriNet station distribution. CDMG stations are shown as squares and USGS/Caltech stations are depicted with triangles. Shading indicates the Quaternary, Tertiary, and Mesozoic (QTM) geologic unit designations of Park and Ellrick (1998) as shown in the legend.

least squares. As the real-time TriNet station density increases, the importance of the centroid will diminish but currently it is imperative for the robust generation of ground motion maps. Fortunately, as planned, TriNet stations are more concentrated in heavily populated regions, so the most reliable recovery of the shaking distribution should be where potential losses and the need for concerted emergency response efforts could be the greatest.

We begin by creating a coarse "rock site" grid (30-km spacing); "phantom" ground motions are assigned to each point on the coarse grid using the Joyner and Boore (1981) distance attenuation relationship for "rock sites" and magnitude of the centroid and its distance to each grid point. These "phantom" ground motion estimates are used to assign shaking values to those points for which there are no nearby TriNet stations (within 30 km). Shaking data from reporting TriNet stations are corrected to "rock site" conditions using a procedure described later and this corrected data is then placed on the coarse "rock site" grid map. The coarse "rock site" grid is next interpolated to a fine "rock site" grid (3-km spacing) which is then corrected for geology. However, shaking at individual stations in this final grid map is the same as that which was actually recorded at the site.

In Figure 2 we show an example of a peak acceleration map for a magnitude 4.4 earthquake near Wrightwood, California (northeast of Los Angeles) which occurred on August 20, 1998. No site corrections have been applied to these maps; however, attenuation with distance and stability to the contour pattern has been assured by the ground motions assigned to the "phantom" stations

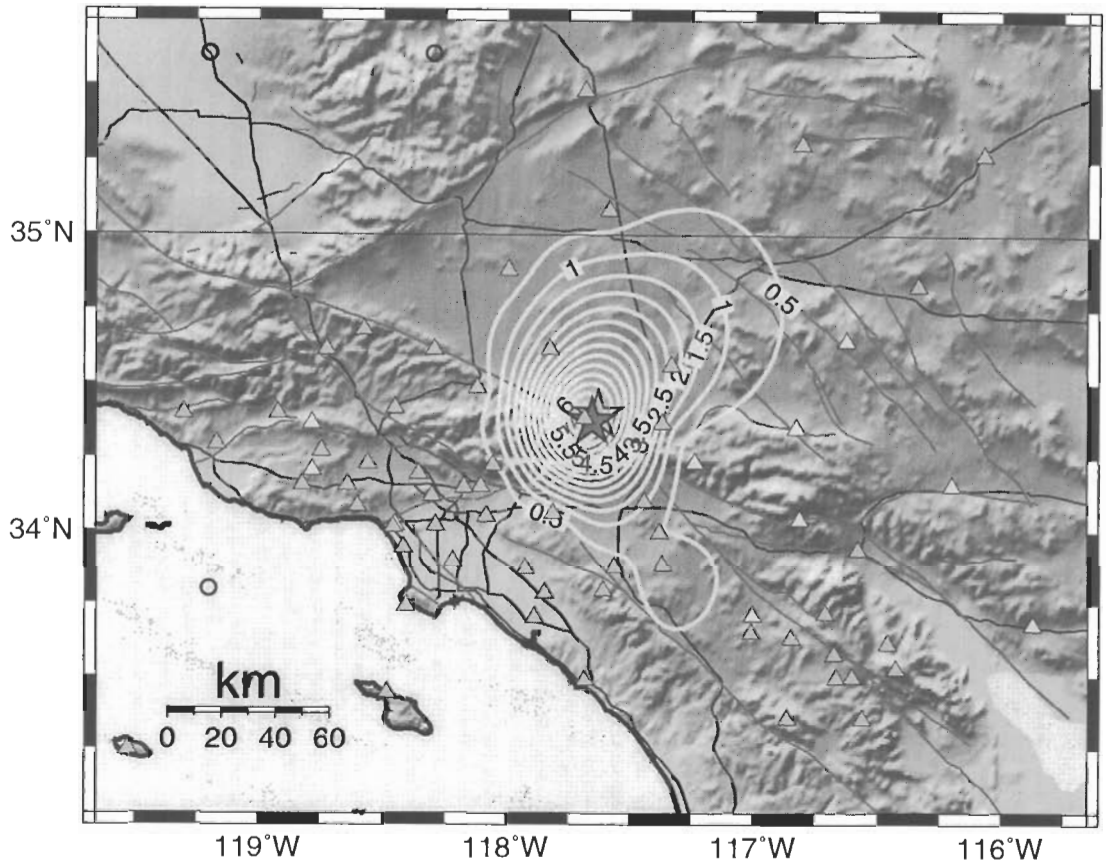

Figure 2: Shaded relief map showing peak accelerations for the August 20, 1998 magnitude 4.4 Wrightwood earthquake with contours of acceleration in percent "g". Lightly shaded triangles represent USGS/Caltech stations; darker shaded triangles represent CDMG stations. Dark lines are freeways and lightly-shaded lines are mapped faults. The shaded star shows the epicenter and the open star represents the strong motion "centroid". Open circles represent "phantom" grid stations (see text for details).

based on the strong motion centroid (M4.4 at location of the open star in Fig. 2) Since this area is fairly well instrumented, there are few "phantom" stations, and the only ones necessary within the map dimensions are depicted (as a open circles) near the eastern edge of the map and in the ocean. All other predicted values in this case are superseded by recorded amplitudes. Out at greater distances, however, more "phantom" stations do contribute and they insure that the contour maps remain well-behaved and bounded at the edges.

SITE CORRECTIONS

In order to interpolate from ground motions recordings on a fairly coarse, non-uniformly spaced network of stations to maps showing continuous functions of ground motion, basic site corrections are useful. For example, direct interpolation between two rock sites surrounding a basin would inadequately represent the true motion within the basin. Hence, we interpolate the data, plus the coarse "grid" stations, onto a finely-spaced (3 km) uniform grid over the entire region. The finely-

interpolated grid has been predefined and so we can preassign a geologically-based site classification to each location.

The amplification correction we use is based on the Quaternary, Tertiary, Mesozoic ("QTM") geological classification of Park and Ellrick (1998). These categories can be considered to represent soil, soft rock, and hard rock, respectively, and hence they provide a very simple but effective way to assign amplification on a regional scale. Based on the average velocities assigned to the QTM categories (Park and Ellrick, 1998), we applied the frequency-and amplitude-dependent amplification factors determined by Borcherdt (1994). Table 1 shows the site amplifications factor for the QTM categories at periods of both 0.3 and 1.0 seconds for each of four input ground acceleration levels. At .3 sec, amplification for the soil (Quaternary Alluvium) sites is nearly a factor of 1.5 at low input motions and it decreases to slightly over 1.0 for strong motions; Tertiary and Mesozoic rock units have a less pronounced amplitude dependency (see Table 1).

Table 1: Site Amplification Factors

Period (sec)	Input Rock Peak Ground Acceleration (gals)			
	<50 gals	50-100 gals	100-200 gals	>200 gals
Mesozoic:				
0.3	1.00	1.00	1.00	1.00
1.0	1.00	1.00	1.00	1.00
Tertiary:				
0.3	1.14	1.10	1.04	0.98
1.0	1.27	1.25	1.22	1.18
Quaternary:				
0.3	1.39	1.15	1.06	0.97
1.0	1.45	1.41	1.35	1.29

We correct the peak acceleration (PGA) amplitude with the 3 Hz amplification factors while the peak velocity (PGV) values are corrected with the 1 Hz factors. The site correction procedure is applied so that the original data values are used to construct the final contours. We then contour the interpolated, site-corrected peak ground acceleration and peak ground velocity values.

Since site amplification factors are considerable at low levels of shaking, applying the site corrections to small earthquakes shows quite noticeable effects. Figure 3 shows a map of the peak accelerations for a magnitude 3.9 earthquake the which occurred in the Imperial Valley on June 26, 1998. The overall pattern of shaking is not well-constrained by the data, in fact this event occurred very near the Mexican border and the edge of the TriNet station coverage. However, a relatively simple pattern of shaking emerges on the contour map. The strong motion centroid (open star) just southeast of the epicenter, is not well constrained in part due to the lack of data to south. Based on this data alone, there is some indication that shaking in the soft-sediment valley floor to the east was greater than to the west, in the mountains. Figure 4 shows the effect of our site correction on the same data set. Note that the shape of the valleys and mountains are clearly delineated, which was not the case with the limited data set alone.

Although only relatively small events have been recorded during the year or so that we have been making "ShakeMap", we can apply the procedure in retrospect to larger earthquakes. In Figure 5 we show a map of the recorded peak velocity distribution (contoured in cm/sec) for the 1994 magnitude 6.7 Northridge earthquake to illustrate the nature of the information provided by

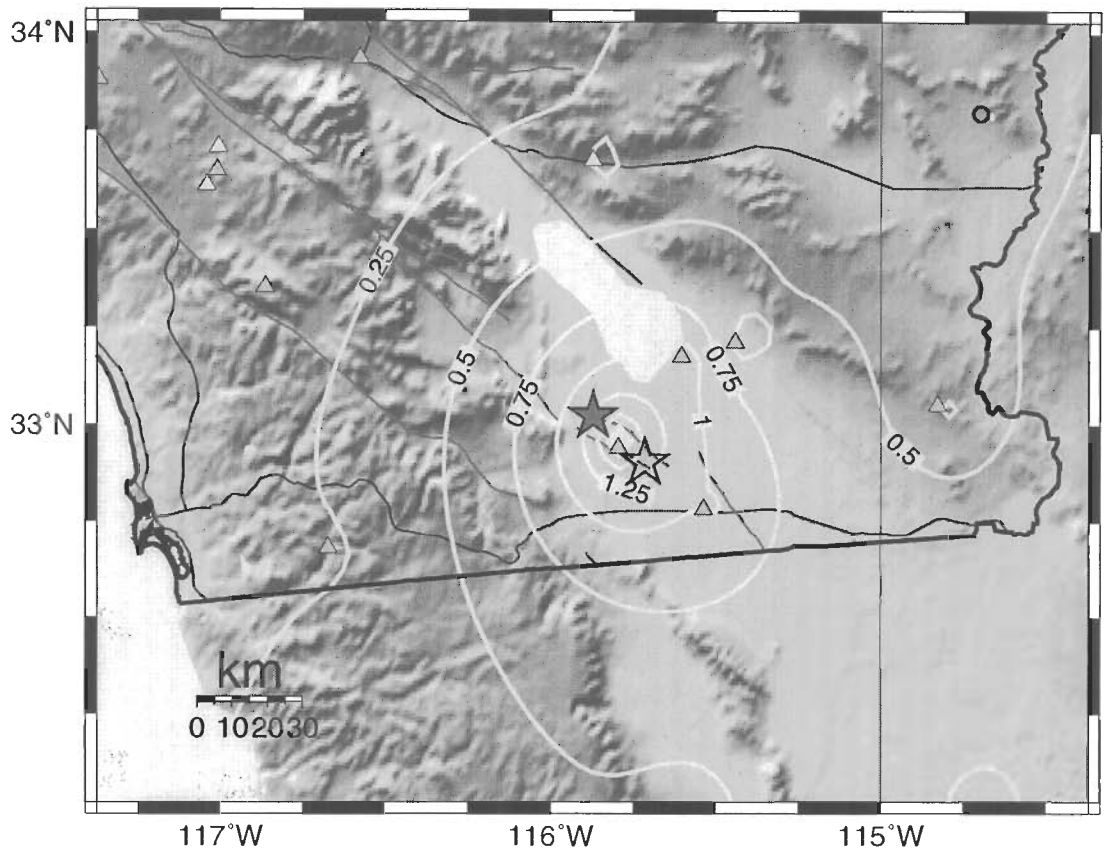

Figure 3: Shaded relief map showing peak acceleration contours for the June 26, 1998 magnitude 3.9 earthquake near Westmorland, California. Contours of are in units %g. No site corrections have been applied. Triangles represent strong-motion stations. The shaded star shows the epicenter and the open star represents the strong motion "centroid".

ShakeMap and the effects of applying the site correction for a larger earthquake. In this particular example, the ground motion data is from existing analog networks (CDMG, USGS, University of Southern California, Southern California Edison, the Los Angeles Department of Water and Power), not the current TriNet digital instrument deployment.

Typically, for moderate-to-large events, the pattern of peak ground velocity reflects the pattern of the earthquake faulting geometry, with largest amplitudes in the near-source region, and in the direction of rupture directivity (Fig. 5). Differences between rock and soil sites are apparent, but the overall pattern is more a reflection of the source proximity and rupture process. Nonetheless, the site effects are important. Based on the tabulated amplification factors (Table 1), we expect that for larger events which are dominated by strong shaking, the effect of site corrections, particularly at high frequencies, are less significant than for the lower shaking levels associated with smaller earthquakes.

The site-corrected peak velocity map for the Northridge earthquake is shown in Figure 6. The differences between the ground velocities within the valleys and surrounding mountains becomes more evident once the site corrections are applied. For example, the overall level of the ground velocities in the San Fernando valley (the "Northridge" label) is higher on the site corrected maps.

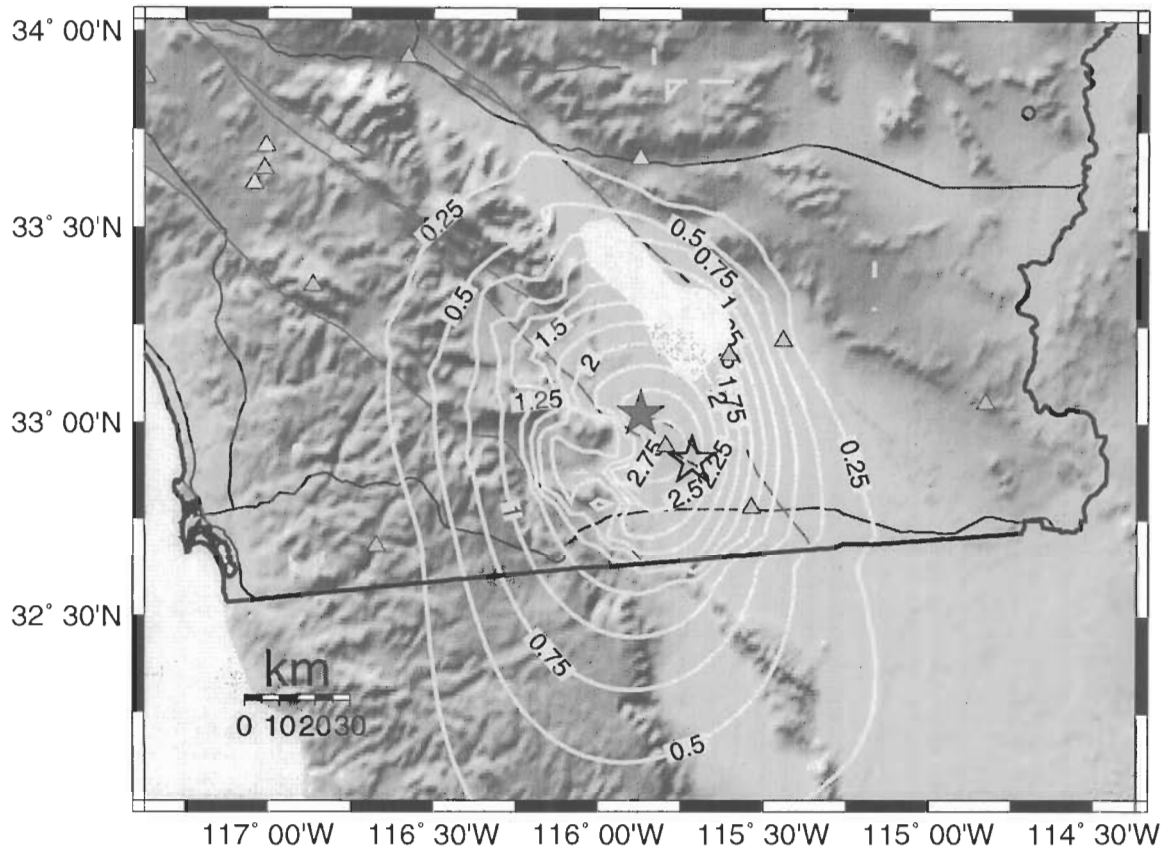

Figure 4: Shaded relief map showing site-corrected peak acceleration contours for the June 26, 1998 magnitude 3.9 earthquake near Westmorland, California. Contours of are in units %g. Triangles represent strong-motion stations. The shaded star shows the epicenter and the open star represents the strong motion "centroid".

In addition, originally smooth contours which simply connected adjacent but distant stations, become more complex when intervening geologically-based site corrections play a role in determining the interpolated amplitudes.

INSTRUMENTAL SEISMIC INTENSITY MAPS

From the PGA and PGV maps, we would like to estimate the ground motion intensity as a simple visual and intuitive way to represent the overall nature of the shaking. Seismic intensity has been traditionally used worldwide as a method for quantifying the shaking pattern and the extent of damage for earthquakes. Though derived prior to the advent of today's modern seismometric instrumentation, seismic intensity nonetheless provides a useful means of describing, in a simplified fashion, the complexity of these same recordings. Such simplification is necessary to grasp the overall extent of the situation for those unfamiliar with the subtleties associated with relating the spatially complex ground motions, which vary as a function of frequency, duration and amplitude, to potential damage.

That is not to say that instrumental intensity alone is sufficient for loss estimation, and in fact, spectral response provides a better physical basis for such analyses. ShakeMap will also provide

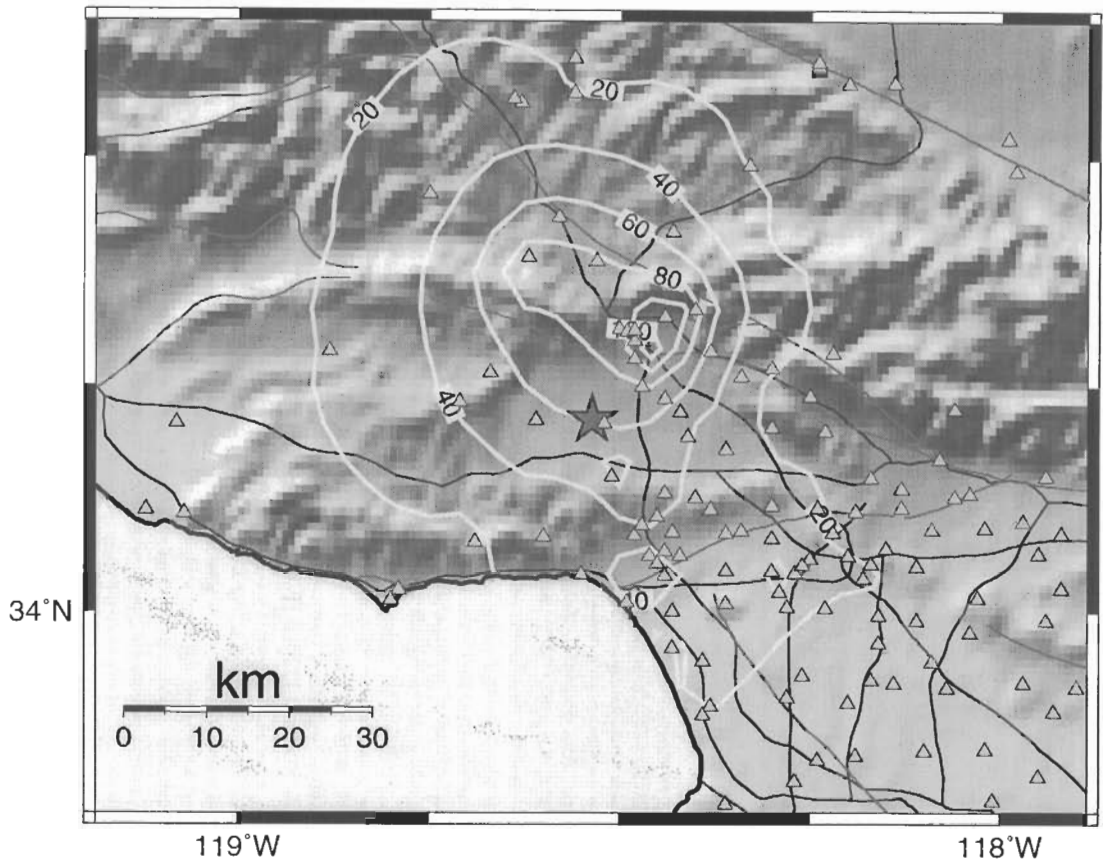

Figure 5: Shaded relief map showing recorded peak velocity contours for the magnitude 6.7 1994 Northridge earthquake. Contours of velocity are in cm/sec. The shaded star shows the epicenter and the open star represents the strong motion "centroid". No site corrections have been applied.

spectral response maps (at 0.3, 1.0, and 3.0 sec), but for the overwhelming majority of users, we feel the intensity map will be more intuitive. Naturally, distilling the complex relationship between spatially highly variable strong ground motions and the potential damage to a wide variety of building construction types in regions of variable building exposure, into a simple-to-use map requires approximation, as does simplifying any complex scientific issue for general understanding. But it is desirable to convey the information in a generally acceptable form.

We have recently developed regression relationships between Modified Mercalli intensity (I_{mm}, Wood and Neumann, 1931, later revised by Richter, 1958) versus PGA and PGV by comparing the peak ground motions to observed intensities for eight significant California earthquakes. The eight events, the 1971 (M6.7) San Fernando, the 1979 (M6.6) Imperial Valley, the 1986 (M5.9) North Palm Springs, the 1987 (M5.9) Whittier Narrows, the 1989 (M6.9) Loma Prieta, the 1991 (M5.8) Sierra Madre, the 1992 (M7.3) Landers, and the 1994 (M6.7) Northridge earthquakes, were used since they were well recorded by regional strong motion networks in addition to having numerous intensity observations (Dewey, written communication, 1997).

Given these events, there is a reasonable overlap between recorded ground motions and the intensity measurements. In earlier studies (e.g., Trifunac and Brady, 1975), similar relations were derived based on taking the intensity value off a map at the location of the strong motion station

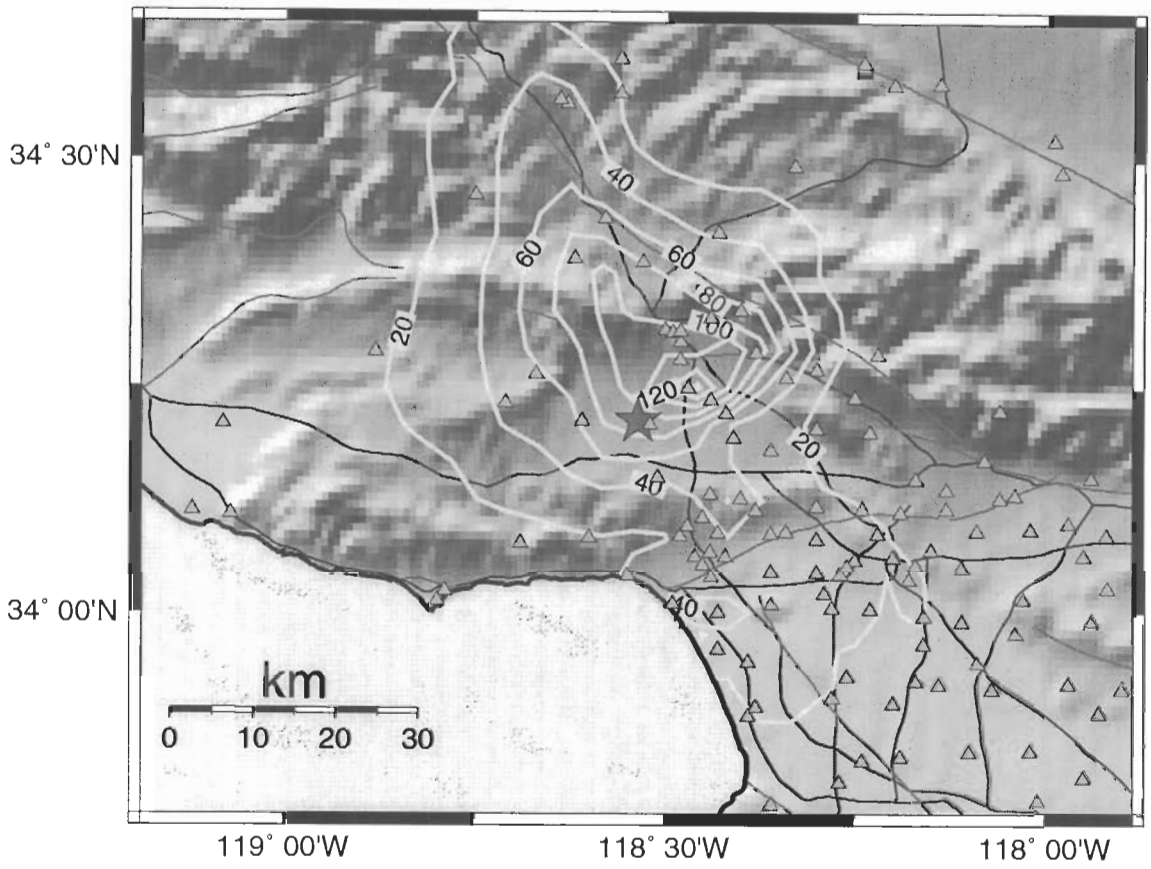

Figure 6: Shaded relief map showing recorded peak velocities, corrected for site amplification, for the magnitude 6.7 1994 Northridge earthquake. Velocity are units of cm/sec. The shaded star shows the epicenter.

when no observation was available near the strong motion site. Since the I_{mm} maps are typically simplified representations of a spatially variable field, the true I_{mm} value at the strong motion recording site is not usually known; there is no guarantee that the I_{mm} at the strong motion station location corresponds with the value I_{mm} value on the map. Here, we chose to correlate only those values where the strong motion station is near (within 3 km) a I_{mm} observation. For each station, the nearest intensity observation is chosen, if no intensity measurement is within 3 km then the strong motion data at that site is not used for correlation purposes. Although ground motions can vary significantly over this distance, requiring more nearly co-located observations reduces the available pairing of data. Since the earlier studies, there is now substantially more strong motion data available, particularly at larger amplitudes, for such a comparison.

Earlier comparisons of peak ground motions and intensities were also based primarily on regressions of intensity against peak acceleration, or in a few cases, against peak velocity. We differ from previous studies in that here we chose to use both peak acceleration and velocity jointly, recognizing the amplitude- and frequency-dependent nature of the intensity scale as manifested by both felt shaking descriptions and actual damage. Figure 7 shows the relationship of I_{mm} values and PGA for the individual events analyzed; Figure 8 shows the same for PGV. Figures 9 and 10 show the regressions of I_{mm} verses and PGA and PGV, respectively, for the data from all eight

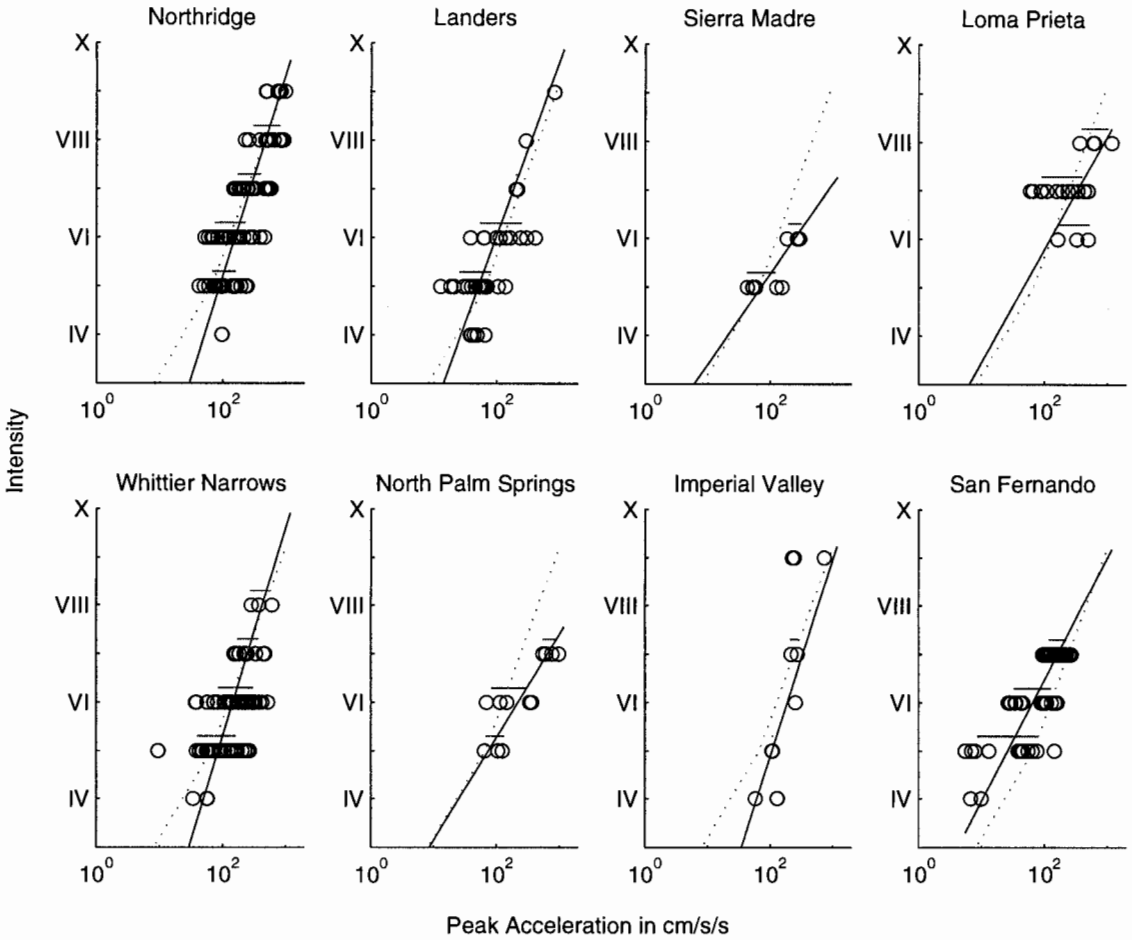

Figure 7: Modified Mercalli intensity plotted against peak ground acceleration for individual earthquakes. Circles denote data, horizontal lines above data depict the range of the geometric mean, plus and minus one standard deviation. Solid line is the regression for individual events; short-dashed line is regression for events combined.

earthquakes combined.

Requiring that the ground motion recording sites and I_{mm} observation points have the same QTM designation, in addition to the maximum distance requirement, did not significantly improve scatter shown in Figures 9 and 10. However, this may be a limitation of the map scale used in the geology classification (1:750,000), and a more detailed association of the geology at the strong motion sites and intensity observations may be useful. Naturally, though, the association of an instrumental, point measurement of ground motion with an intensity observation defined as an average over a designated areal extent would be expected to show substantial scatter, particularly if the area does not even contain the point measurement. This is a fundamental limitation originating from the definition of seismic intensity which requires an (unspecified) area be assigned an given intensity value based on the representative or average level of damage in the specified region. Any single point observation in that area is not sufficient to satisfy such a definition.

While there is no fundamental reason to expect a simple relationship between Modified Mercalli

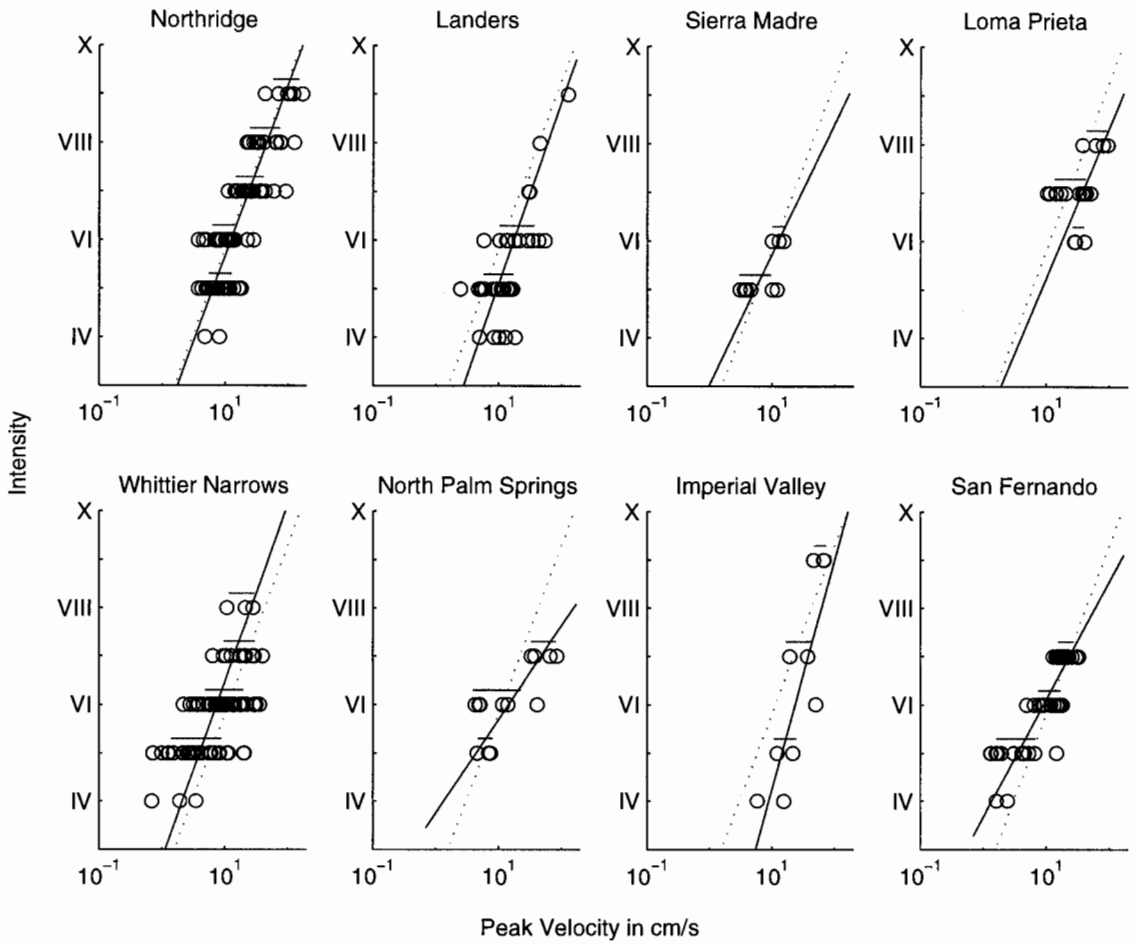

Figure 8: Modified Mercalli intensity plotted against peak ground velocity for individual earthquakes. Circles denote data, horizontal lines above data depict the range of the geometric mean, plus and minus one standard deviation. Solid line is the regression for individual events; short-dashed line is regression for events combined.

intensity and recorded ground motion parameters, over a range of accelerations and velocities a simple power-law representation is adequate and convenient. For the limited range of Modified Mercalli intensities (I_{mm}), we find that for peak acceleration (PGA) with V $\leq I_{mm} \leq$ VIII,

$$I_{mm} = 3.56log(PGA) - 1.48 \quad (1)$$

and for peak velocity (PGV) with V $\leq I_{mm} \leq$ IX,

$$I_{mm} = 3.48log(PGV) + 2.32 \quad (2)$$

Here the regressions are made on the geometric mean of the peak ground motion values for a given intensity value. For acceleration, I_{mm} IX is not used in the regression since the peak acceleration values appear to be saturated, and as such a simple power-law relation will not suffice. Likewise at I_{mm} IV, peak accelerations may be biased high due to lack of digitization of data from

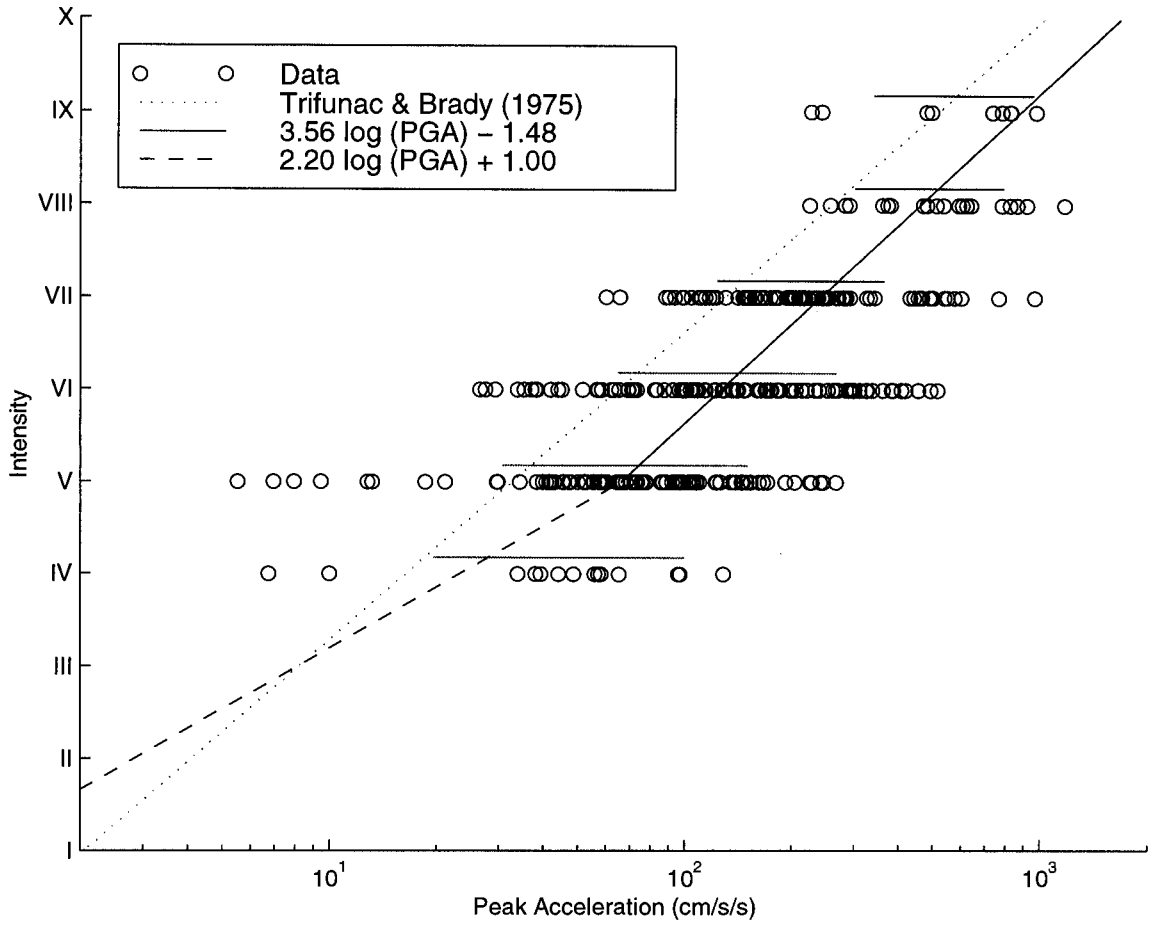

Figure 9: Modified Mercalli intensity plotted against peak ground acceleration for all events combined. Circles denote data; horizontal lines above data depict the range of the geometric mean, plus and minus one standard deviation. Solid line is regression from this study; short-dashed line is that of Trifunac and Brady (1975).

station with lower values and so they are not used in the regression. For $I_{mm} \leq$ IV, peak velocities do not continue decreasing, suggesting perhaps not only the above-mentioned bias, but also a higher noise level (likely introduced in the integration of digitized recordings) may be controlling the peak values; hence, those values are not used in the regression.

Since we are defining intensity at lower values by the peak acceleration value, and our current collection of data from historical earthquakes does not provide constraints for lower intensity, we have imposed the following relationship between PGA and I_{mm}:

$$I_{mm} = 2.20log(PGA) + 1.00 \tag{3}$$

This basis for the above relationship comes from correlation of TriNet peak ground motions recordings for recent magnitude 3.5 to 5.0 earthquakes with intensities derived from voluntary response from Internet users (Quitoriano *et al.*, 1998) for the same events. We determined that the boundary between "not felt" and "felt" (I_{mm} I and II, respectively) regions corresponds to

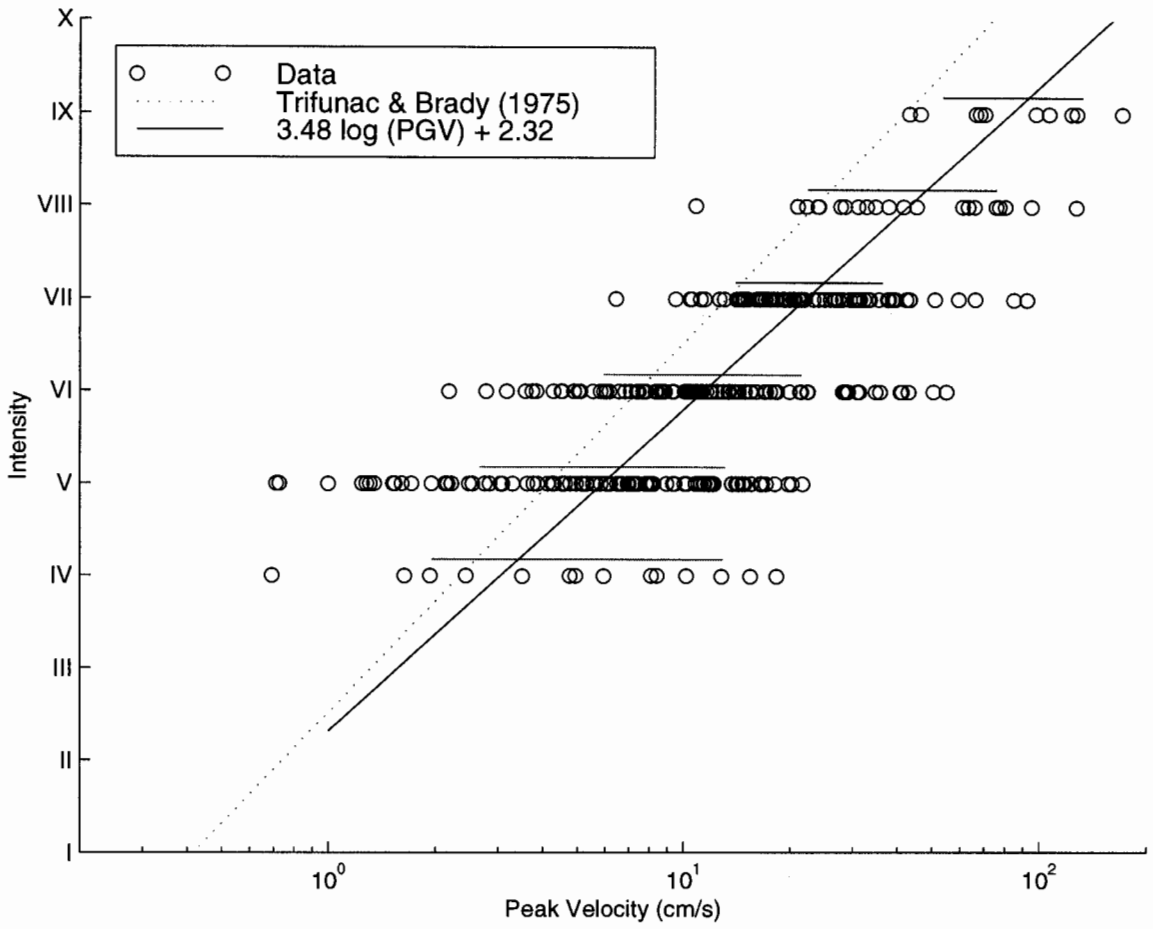

Figure 10: Modified Mercalli intensity plotted against peak ground velocity for all events combined. Circles denote data; horizontal lines above data depict the range of the geometric mean, plus and minus one standard deviation. Solid line is regression from this study; short-dashed line is that of Trifunac and Brady (1975).

approximately one to two cm/sec/sec, at least for this range of magnitudes. We then assigned the slope such that the curve would intersect the relationship in equation 1 at I_{mm} V. We plan to refine this as more digital data becomes available.

For a given ground motion level, our intensities are are higher compared to the commonly used relationships of Trifunac and Brady (1975), which is also displayed on Figures 9 and 10. Only data from the 1971 San Fernando earthquake are common; our data is from 1971 forward, while that of Trifunac and Brady (1975) contains prior earthquakes. In general, the main differences are due to the addition of new data since the Trifunac and Brady (1975) study. However, for acceleration, part of the difference is that we do not include the intensity IX (or larger) values in the regression, due to the evidence of amplitude saturation, whereas Trifunac and Brady (1975) used an intensity X value. Likewise, for velocity, we did not use lower intensity values ($I_{mm} \leq$ IV) for the regression whereas Trifunac and Brady (1975) did so.

It is notable that relations of Trifunac and Brady (1975) were substantially higher (stronger motions required for a given intensity) than most earlier estimates (see Trifunac and Brady, 1975,

Figure 3), and now our relationship indicates yet higher ground motions associated with the same intensity levels. There are a number factors that may influence this trend, and certainly more densely spaced recordings in the near-fault region of the recent events, particularly for the Northridge earthquake, does presumably favor a more accurate portrayal of the relationship. However, building practices have certainly improved since the earlier events studied, altering the association of shaking and damage. There are fewer brittle structures that are easily damaged at moderate levels of ground acceleration. Hence, it may be natural that such empirical relationships change with time.

As seen in Figures 9 and 10, low levels of shaking intensity correlate best with peak acceleration, while high intensities correlate best with peak velocity. Basically, peak acceleration levels off at high intensity while peak velocity continues to grow. In contrast the ground velocities, derived by integration of digitized analog accelerograms, are noisy at low levels of motion so a meaningful correspondence is elusive. By comparing maps of instrumental intensities with I_{mm} for the eight above-mentioned earthquakes, we have found that a relationship that follows acceleration for I_{mm}<VII and follows velocity for I_{mm}>VII works fairly well. In practice, we compute the I_{mm} from the I_{mm} verses PGA relationship; if the intensity value determined from peak acceleration is $\geq$ VII, we then use the value of I_{mm} derived from the I_{mm} verses PGV relationship.

This is intuitively consistent with the notion that lower (<VI) intensities are assigned based on felt accounts, and people are more sensitive to ground acceleration than velocity. Higher intensities are defined by the level of damage; the onset of damage at the intensity VI to VII range is usually characterized by brittle-type failures (masonry walls, chimneys, unreinforced masonry, etc.) which are sensitive to higher-frequency accelerations. With more substantial damage (VII and greater), failure begins in more flexible structures, for which peak velocity is more indicative of failure (e.g., Hall *et al.*, 1996).

Table 2 gives the peak ground motions that correspond to each unit Modified Mercalli intensity value according to our regression of the observed peak ground motions and intensities for California earthquakes. By relating recorded ground motions to Modified Mercalli intensities, we can now estimate shaking intensities within a few minutes of the event based on the recorded peak motions made at seismic stations. Note that the estimated intensity map is derived from ground motions recorded by seismographs and represents intensities that are likely to have been associated with the ground motions. However, unlike conventional intensities, the instrumental intensities are not based on observations of the earthquake effects on people or structures. Further, the range of peak values for a given intensity is likely to change as additional data sets are included.

Table 2: Relationship of Peak Ground Motions to Intensities

Intensity	I	II-III	IV	V	VI	VII	VIII	IX	X+
Perceived Shaking	Not Felt	Weak	Light	Moderate	Strong	Very Strong	Severe	Violent	Extreme
Damage	None	None	None	Very Light	Light	Moderate	Moderate to Heavy	Heavy	Very Heavy
Peak Acc. (% g)	<0.17	0.17-1.4	1.4-4.0	4.0-9.3	9.3-18	18-34	34-65	65-124	>124
Peak Vel. (cm/s)	<0.6	0.6-2.2	2.2-4.2	4.2-8.2	8.2-16	16-31	31-60	60-114	>115

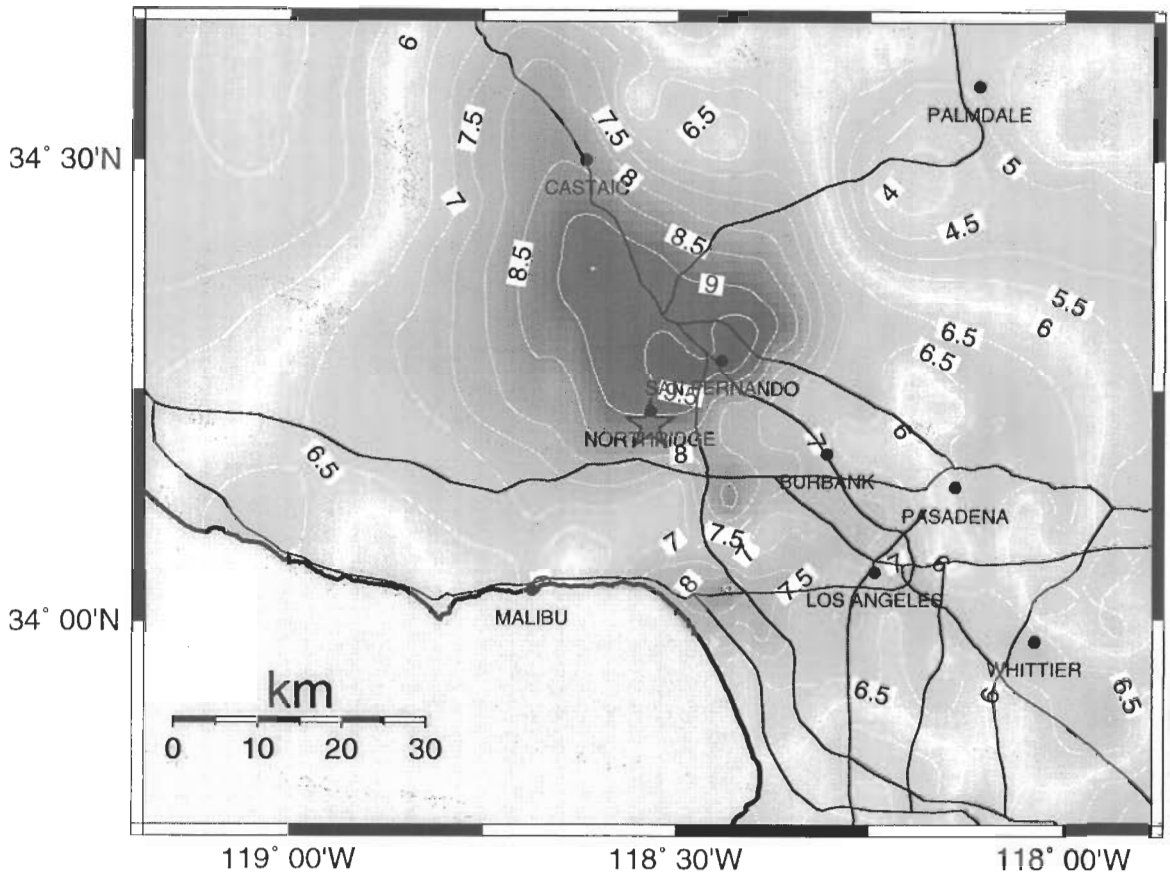

INTENSITY	I	II-III	IV	V	VI	VII	VIII	IX	X+
Perceived Shaking	Not felt	Weak	Light	Moderate	Strong	Very strong	Severe	Violent	Extreme
DAMAGE	none	none	none	Very light	Light	Moderate	Moderate/Heavy	Heavy	Very Heavy
PEAK ACC.(%g)	*<0.17*	*0.17-1.4*	*1.4-4.0*	*4.0-9.3*	*9.3-18*	18-34	34-65	65-124	>124
PEAK VEL. (cm/s)	<0.6	0.6-2.2	2.2-4.2	4.2-8.2	8.2-16	*16-31*	*31-60*	*60-115*	*>115*

Figure 11: Instrumental intensity map for the 1994 Northridge earthquake derived using the procedure outlined in the text. Shading corresponds to the intensity scale in the legend at the bottom of the figure. The epicenter is shown with a filled star, Black lines depict highways. Small circles show selected city locations as labeled. Also given in the scale bar are corresponding peak ground motion values, one- or two-word shaking and damage descriptors (See also Table 1).

Figure 11 shows the site-corrected, instrumental intensity map derived using the procedure outlined above using strong motion data recorded during the Northridge earthquake. The epicenter is shown with a solid star and black lines depict highways. The shading corresponds to the intensity scale shown below the figure, and two-word descriptions of both shaking and damage levels are provided (L. Dengler and J. Dewey, written communication, 1998). On the World Wide Web version of the maps, rather than contour lines, the shading is color-coded, with yellow, orange and red representing increasing levels of potential damage. Given the current station distribution, we can recover approximately the Northridge intensity map (Fig. 11) if the CDMG dialup data is included (1/2 hour). This map shares most of the notable features of the Modified Mercalli map prepared by Dewey *et al.* (1995). The area of I_{mm} IX on the instrumentally-derived intensity map is greater in comparison with the Dewey *et al.* (1995) map. This reflects the fact that although much of the regions in the Santa Susanna mountains, north and northwest of the epicenter, were very strongly shaken, the region is also sparsely populated. Hence the observed intensities were not represented. This is a fundamental difference between observed and instrumentally-derived intensities.

Though there is some degradation when the 5-minute map is made using only the USGS/Caltech real-time stations, it nonetheless provides for more information that was available in the early morning of January 17, 1994. In that case it took over one half an hour to provide just the epicenter and magnitude. Had this map been available in the minutes following the Northridge earthquake, much more would have been understood about the scope of the disaster and the variations in damage over the Los Angeles metropolis.

Initially, our use of PGA and PGV for estimating intensities was simply practical. We were only retrieving peak values from a large subset of the network, so it was impractical to compute more specific ground motion parameters, such as average response spectral values, kinetic energy, cumulative absolute velocities (CAV, EPRI, 1991), or the JMA algorithm (Japan Meteorological Agency, 1996). However, we find the use of PGA and PGV to be quite suitable, particularly since near-source ground motions recorded during these earthquakes are nearly always dominated by short-duration, pulse-like characteristics usually associated with source directivity, and these are by far the largest motions. In other words, for the many of the most damaging ground motions, the kinetic energy available for damage can be well characterized by the peak velocity value. The close correspondence of the JMA intensities and peak ground velocity (Kanezashi and Kaneko, 1997) indicates that our use of peak ground velocities for higher intensities is consistent with the algorithm used by JMA. Another consideration in the choice of peak ground motion values, rather than derived parameters, is the ease in then relating intensity directly to simple ground motion observables.

For large distant earthquakes, the peak values will be less informative, and duration and spectral content will become key parameters. While eventually we may adopt corrections for these situations, it is difficult to assign intensities in such cases. For instance, what is the intensity in the zone of Mexico City from the 1985 Michoacan earthquake, where numerous high-rises collapsed, but the overwhelming majority of smaller buildings were unaffected? While the peak ground velocities were moderate and would imply I_{mm} VIII, resonance and duration conspired to cause a more substantial disaster. Although this is, in part, a shortcoming of using peak parameters alone, it is more a limitation imposed by simplifying the complexity of ground motions into a single parameter. As such, in addition to providing peak ground motion values and intensities, we will be producing spectral response maps as well (for 0.3, 1.0, and 3.0 sec), and those users that can take advantage of this information for loss estimation will have a clearer picture than intensity and peak ground motion values alone can provide. However, as discussed earlier, a simple intensity map is extremely useful for the overwhelming majority of the users, which includes the general public and many

involved with the initial emergency response.

The use of PGV for higher intensities also proves important for several cases for which we have recorded a large, single-spike of high-frequency acceleration recorded for small earthquakes. With our procedure, while the large acceleration peak would provide an abnormally high intensity, the much smaller velocity amplitude provides a more appropriate, lower intensity. In contrast small earthquakes, which are nonetheless widely felt in many areas of southern California, generally provide rather noisy velocity recordings and hence the estimation of intensity from them alone is less reliable. For smaller events, acceleration amplitudes provide more reliable intensity estimates though there are currently few data constraining the lowest intensity levels.

THE SHAKEMAP WEB PAGE

After triggering, events are automatically processed, added to the database and are made available through the World Wide Web online interface. The Web site provides access to not only maps of recent earthquakes (for instance, a mainshock and significant aftershocks), but also historical events processed to provide a basis for comparison with recent events. The actual processing of the peak acceleration, peak velocity, and intensity maps, including printing and complete Web page generation, takes less than one minute once triggered for the uncorrected maps; site corrections take an additional minute.

The maps as viewed on the Web are interactive imagemaps. Selection of individual stations on the map initializes a lookup table that provides station information, including station names, coordinates, and the peak ground motions values recorded on each component. Such information has been greatly sought following major earthquakes but only now can it be provided in a rapid fashion.

For significant events (e.g., magnitude greater than 5.0), full-color, poster-sized maps are also generated automatically. In addition, a first motion mechanism (e.g., Reasenberg and Oppenheimer, 1975) and rapid moment tensor solution (Thio and Kanamori, 1995), both automatically generated, are added to the ShakeMap Web page as they are received to provide additional information about the nature of the earthquake source. Summary files are also generated for each data set to be used for distribution. These files include the raw data, interpolated and site-corrected grid files and the values of the contour lines used on the maps.

DISCUSSION

With the QTM designation, we can get a large component of the total amplification effect with a small number of parameters. More importantly, these simple, geological classifications are available over the whole of southern California. A compilation of more localized (and better constrained) site corrections based on either shallow soil velocity profiles or mainshock/aftershock studies (e.g., Hartzell *et al.*, 1998) may improve the interpolation technique that we currently use. However, such data is not uniformly available and a new technique would have to be developed to incorporate such subsets into the interpolation scheme. Further, the effects of soil nonlinearity are not quantified in such site response maps since a majority of the ground motions are at low levels of input motion, and these effects could be important at the strong motion levels for which we anticipate ShakeMap will be most useful.

One implication of using site-corrections that depend on frequency and amplitude, which clearly reflect nonlinearity at large motions, is that the site corrections become smaller as amplitudes increase into the nonlinear range. Arguably, this range is for peak accelerations above 15-20% "g" (e.g, Beresnev and Wen, 1996; Field *et al.*, 1997). As seen in Table 1, both the 1 and 3 Hz site

corrections are rather small above 200 gals, so the site correction has only a minor effect for intensity VII or greater (which are based on the peak velocity, or 1 Hz, correction factors). However, with any moderate-to-large earthquake, it will be important to delineate the boundaries of potentially damaging strong motions and those regions moderately shaken at greater distances from the source.

The current site corrections being used are clearly only first order corrections. The QTM geology is highly simplified; shallow Quaternary alluvium sites can behave as bedrock; likewise, some digital stations mapped on rock indicate substantial observed site amplifications. We have not yet addressed the potential for severe site effects and liquefaction in areas of southern California with extremely slow surface shear wave velocities (NEHRP category D) such as in the Los Angeles Harbor region and along former and current river channels. Not only are we limited by the lack of sufficiently detailed geologic maps of such areas, but the connection between the surface geology and the site amplification is not fully established for strong motions. Similarly, basin edge effects are not included, and differences between very deep basin and shallow basin sites are not yet distinguished. In addition, only peak values have been consider here; site resonance is not yet considered. Shaking duration has also not yet been included, though it may be an important under certain circumstances. For instance, at this point we would likely underestimate the extent of damage (intensity) in Los Angeles for a great San Andreas event since only peak amplitude is considered, but currently there is little empirical constraint upon which to base a modification to the instrumental intensity computation for such an event. For such an earthquake, evaluation of the response spectral map would be crucial.

CONCLUSIONS

The peak ground motion versus intensity correlation is based on observations collected from recent California earthquakes. Hence, although intended to correspond with observations, as more data become available, this parameterization is subject to revision as necessary to accommodate additional observations as well as changes in building practice. The seismic intensities we produce immediately following damaging earthquakes are based on recorded ground motions; they are not based on observed phenomena usually associated with seismic intensities. Although intended to correspond, locations of equal instrumental intensity may suffer different degrees of damage based on both the density and type of structures and the exact nature of the ground motions.

At present, there is little data to correlate lower intensity values and recorded ground motions since most of the ground motion data is for larger earthquakes, and intensity data is not typically collected for smaller events. In addition, the calibration we have is primarily for analog recordings, so the noise level is high, especially for low amplitude (once-integrated) velocity seismograms. The digital data now being collected with TriNet will be more useful in calibrating against intensity at lower amplitudes. TriNet will provide low amplitude ground motion recordings, previously unavailable with triggered, analog stations. In addition, we are also collecting intensity measurements at near-station locations through voluntary response on the Internet (Quitoriano *et al.*, 1998) (URL*http://www-socal.wr.usgs.gov/ciim.html*). The combination of assigning intensities for low shaking levels with digital recordings will help constrain the relationship between acceleration and intensity at the lowest values.

Naturally, we are most concerned about accurately portraying the highest intensities. For example, due to the Northridge earthquake, approximately 86% of the residential losses occurred in the intensity VII-IX region (Kircher *et al.*, 1997, p 714). Intensity IX was the largest mapped value for that event. Interestingly, though, while the main emphasis of "ShakeMap" is to provide information about shaking for damaging earthquakes where the pattern of shaking can be quite complex, there has been widespread interest in viewing maps for smaller earthquakes which are,

nonetheless, widely felt. We generate "ShakeMap" for all earthquakes in southern California above magnitude 3.0, but we only update the Web pages for magnitude 3.9 and greater, since the felt area for the smaller events is usually nominal. However, for several notable earthquakes in the 3.0 to 3.9 range, there has been a substantial demand for rapid display of the shaking pattern and so we have provided maps for these events as well. The advantage in providing ShakeMap for non-damaging earthquakes is twofold. First, we gain experience processing, calibrating, and checking our system by responding to small events daily to weekly, rather than on the very infrequent basis allowed by the occurrence of moderate to large earthquakes. Second, the user groups (which includes emergency response agencies, utilities, the media, scientists, and the general public) are afforded the opportunity to become familiar with the maps and to test their response on a more regular basis.

A critical component in successfully generating "ShakeMap" is a system that is robust; that is, it must function under the adverse conditions present during a damaging earthquake including strong shaking of computer equipment, power failures, communication problems, Internet bottlenecks, etc. Efforts have been ongoing to address these concerns. The generation of ShakeMap will provide a much clearer picture of the nature and extent of ground movement following the next significant southern California earthquake and will provide a sound starting point for immediate loss estimation. The World Wide Web uniform resource locator for the "ShakeMap" is *http://www.trinet.org/shake.html*

ACKNOWLEDGMENTS

Conversations with J. Boatwright, R. Borcherdt, L. Dengler, J. Dewey, J. Goltz, K. Campbell, R. Nigbor, and M. Petersen were very helpful. Jim Dewey provided the intensity data in digital form. S. Park provided his QTM geology maps in digital form. All the participants in TriNet played a critical role in making this happen, most notably D. Given, E. Hauksson, P. Maechling, and A. Shakal. Maps and significant portions of the interpolation processing is done with Generic Mapping Tools (GMT, Wessel and Smith, 1991).

REFERENCES

Beresnev, I. A., and K.-L. Wen (1996). Nonlinear soil response - a reality? (A review), *Bull. Seism. Soc. Am.*, **86**, 1964-1978.

Borcherdt, R. D. (1994). Estimates of site-dependent response spectra for design (methodology and justification), *Earthquake Spectra*, **10**, 617-654.

Dewey J. W., B. Glen Reagor, L. Dengler, and K. Moley (1995). Intensity distribution and isoseismal maps for the Northridge, California, earthquake of January 17, 1994, *U. S. Geological Survey Open-File Report* **95-92**, 35 pp.

Eguchi, R. T., J. D. Goltz, H. A. Seligson, P. J. Flores, T. H. Heaton, and E. Bortugno (1997). Real-time loss estimation as an emergency response descision support system: The Early Post-Earthquake Damage Assessment Tool (EPEDAT), *Earthquake Spectra*, **13**, 815-832.

EPRI (1991). Standardization of cumulative absolute velocity, EPRI TR100082 (Tier 1), Palo Alto, California, Electric Power Research Institute, prepared by Yankee Atomic Electric Company.

Field, E. H. P. A. Johnson, I. A. Beresnev, and Y. Zheng (1997). Nonlinear sediment amplification during the 1994 Northridge earthquake, *Nature*, **390**, 599-602.

Hall, J. F., T. H. Heaton, M. W. Halling, and D. J. Wald (1996). Near-source ground motions and its effects on flexible buildings, *Earthquake Spectra*, **11**, 569-606.

Hartzell, S. H., S Harsen, A. Frankel, D. Carver, E. Cranswick, M. Meremonte, and J. Michael (1998) First-generation site response maps for the Los Angeles region based on earthquake ground motions, *Bull. Seism. Soc. Am.*, **88**, 463-472.

Japan Meteorological Agency (1996). Note on the JMA seismic intensity, JMA report 1996, *Gyosei* (in Japanese).

Joyner, W. B. and Boore, D. M. (1981). Peak horizontal accelerations and velocity from strong-motion records including records from the 1979 Imperial Valley, California, earthquake, *Bull. Seism. Soc. Am.* **71**, 2011-2038.

Kanamori, H. (1993). Locating earthquakes with amplitude: Application to real-time seismology, *Bull. Seism. Soc. Am.* **83**, 264-268.

Kanezashi, S., and F. Kaneko, (1997). Relations between JMA's measuring seismic intensity (MI) and phyical parameters of earthquake ground motion, *OYO Tenical Report, 1997*, 85-96.

Kircher, C. A., R. K. Reitherman, R. V. Whitman, and C. Arnold, 1997. Estimation of earthquake losses to buildings, *Earthquake Spectra*, bf 13, 703-720.

Mori, J., H. Kanamori, J. Davis, E. Hauksson, R. Clayton, T. Heaton, L. Jones, and A. Shakal (1998). Major improvements in progress for southern California earthquake monitoring, *Eos Trans. AGU*, **79**, p. 217,221.

Park, S. and S. Ellrick (1998). Predictions of shear wave velocities in southern California using surface geology, *Bull. Seism. Soc. Am.*, **88**, 677-685.

Quitoriano, V., D. J. Wald, L. Dengler, and J. W. Dewey (1998). Utilization of the Internet for Rapid Community Seismic Intensity Maps, *Eos Trans. AGU*, **79**, in press.

Reasenberg, P., and D. Oppenheimer (1975). FPFIT, FPPLOT, and FPPAGE: Fortran programs for calculating and displaying earthquake fault plane solutions, *U. S. Geological Survey Open-File Report* **75-739**, 109 pp.

Richter, C.F. (1958). Elementary Seismology. W. H. Freeman and Company, San Francisco, pp. 135-149, 650-653.

Shakal, A., C. Peterson, A. Cramlet, and R. Darragh (1996). Near-real-time CSMIP strong motion monitoring and reporting for guiding event response, in *Proceedings of the 11th World Conference on Earth. Eng.*, Acapulco, Mexico.

Shakal, A., C. Peterson, and V. Grazier (1998). Near-real-time strong motion data recovery and automated processing for post-earthquake utilization, *Sixth Nat'l Conference on Earth. Eng.*, Seattle.

Thio, H. K., and H. Kanamori (1995). Moment tensor inversion for local earthquakes using surface waves recorded at TERRAscope, *Bull. Seism. Soc. Am.* **85**, 1021-1038.

Trifunac, M. D., and A. G. Brady (1975). On the correlation of seismic intensity scales with the peaks of recorded ground motion, *Bull. Seism. Soc. Am.* **65**, 139-162.

Wald, D. J., T. Heaton, H. Kanamori, P. Maechling, and V. Quitoriano (1997). Research and Development of TriNet "Shake" Maps, *Eos Trans. AGU*, **78**, No. 46, p F45.

Wessel, P. and Smith, (1991). Generic Mapping Tools, *Eos Trans. AGU* **72**, 441.

Wood, H. O. and Neumann (1931). Modified Mercalli intensity scale of 1931, *Bull. Seism. Soc. Am.* **21**, 277-283.

Yamakawa, K. (1998). The Prime Minister and the earthquake: Emergency Management Leadership of Prime Minister Marayama on the occasion of the Great Hanshin-Awaji earthquake disaster, *Kansai Univ. Rev. Law and Politics*, **No. 19**, 13-55.